

Importance-Aware Activation-Space Reconstruction

Md Mokarram Chowdhury*

Department of Computer Science, Iowa State University, United States

MOKARRAM@IASTATE.EDU

Daniel Agyei Asante

Department of Computer Science, Iowa State University, United States

DASANTE@IASTATE.EDU

Ernie Chang

AI at Meta, United States

ERNIECYC@META.COM

Yang Li*†

Department of Computer Science, Iowa State University, United States

YANGLI1@IASTATE.EDU

Editor:

Abstract

Large language models (LLMs) achieve strong performance across many domains but are difficult to deploy in resource-constrained settings due to their size. Low-rank weight matrix compression is a popular strategy for reducing model size, typically by minimizing weight reconstruction error under the assumption that weights are low-rank. However, this assumption often does not hold in LLMs. Instead, LLM activations exhibit stronger low-rank structure—prompting a shift toward minimizing activation reconstruction error.

We show that this shift alone is insufficient: activation dimensions contribute unequally to model performance, and uniform reconstruction can harm performance. We propose IMPACT, a principled framework for importance-aware activation reconstruction that links model compression decisions to their impact on model behavior. IMPACT formulates an optimization problem that considers both activation structure and gradient sensitivity, and derives a closed-form solution where the optimal reconstruction bases are the eigenvectors of an importance-weighted activation covariance matrix. This enables low-rank approximations explicitly optimized to preserve accuracy. Experiments across diverse models and tasks show that IMPACT achieves up to 48.6% greater model size reduction with accuracy comparable to state-of-the-art baselines.

Keywords: large language model, model compression, low-rank approximation, activation sensitivity, efficient inference

1 Introduction

Large language models (LLMs) have achieved remarkable success across a wide range of domains. However, their massive size poses a significant barrier to deployment, particularly in resource-constrained environments. Larger models require more memory, incur slower token throughput, and demand greater computational resources during inference. As a result, there is growing urgency to develop compression techniques that can reduce model size while preserving performance.

*. Equal contribution

†. Corresponding author. Address: 2434 Osborn Dr, Ames, IA 50011, United States.

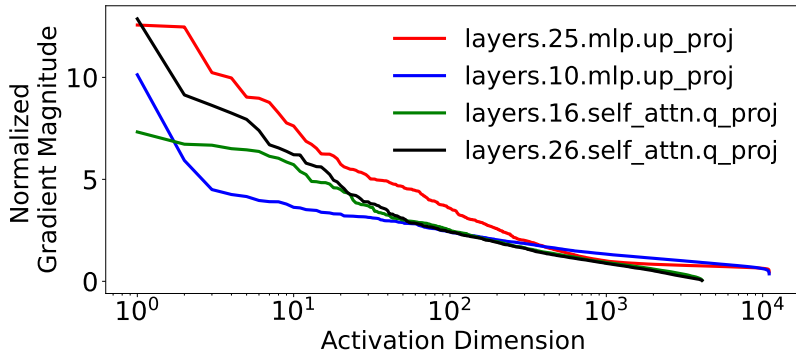


Figure 1: Normalized average gradient magnitudes across activation dimensions in Llama 2-7B on a mathematical reasoning task. For each linear layer, the output activation is a vector $\mathbf{y} \in \mathbb{R}^d$, where each component y_i is referred to as an activation dimension. Dimensions are sorted in descending order by their normalized squared gradient magnitude, which indicates their relative contribution to the loss. The gradient magnitudes vary substantially across activation dimensions—a pattern also consistently observed in other models and tasks.

Low-rank weight matrix compression has emerged as a widely-used strategy for model compression (Xue et al., 2013; Acharya et al., 2019; Noach and Goldberg, 2020; Huang et al., 2021; Lv et al., 2023; Sharma et al., 2024). It approximates a weight matrix $\mathbf{W} \in \mathbb{R}^{m \times n}$ as the product of two smaller matrices, $\mathbf{W}_1 \in \mathbb{R}^{m \times k}$ and $\mathbf{W}_2 \in \mathbb{R}^{k \times n}$, where $k \ll m, n$, thereby reducing the number of parameters. Classical methods select \mathbf{W}_1 and \mathbf{W}_2 to minimize the reconstruction error $\|\mathbf{W} - \mathbf{W}_1\mathbf{W}_2\|$, implicitly assuming that the weight matrix itself is low-rank.¹ However, recent evidence from Yu and Wu (2023) reveals that the weight matrices in large-scale models are often not low-rank, limiting the efficacy of direct weight approximation. Interestingly, they observe that the *activations*—the outputs of linear layers—tend to exhibit much stronger low-rank structure. This has led to a shift in focus: instead of minimizing weight reconstruction error, some recent methods (Yu and Wu, 2023; Chen et al., 2021b) minimize the error in reconstructing the activations induced by those weights, achieving better empirical performance.

However, minimizing activation reconstruction error alone is insufficient to guarantee strong model performance. As shown in Figure 1, different activation dimensions vary widely in their influence on the loss: dimensions associated with large gradients are highly sensitive to reconstruction errors, whereas others contribute little even when poorly reconstructed. Thus, treating all dimensions equally during compression can disproportionately harm those that matter most—leading to greater performance degradation despite low reconstruction error. This raises a critical question:

How can we align activation reconstruction decisions with their actual performance impact?

Answering this question requires a principled framework that explicitly connects weight compression, activation reconstruction, and their contribution to the model performance—a

1. The rank of a matrix is the number of linearly independent rows or columns. A low-rank matrix allows for a small k with minimal reconstruction error.

connection that has not yet been systematically explored in the context of low-rank weight matrix compression.

To this end, we propose IMPACT, a theoretical framework that guides importance-aware activation space reconstruction. IMPACT rigorously analyzes the relationship among weight compression, activation reconstruction, and model performance. By explicitly linking reconstruction decisions to their performance impact, it provides principled guidance for selecting weights to minimize performance degradation. The framework is grounded in a formal optimization formulation, which is transformed into a more tractable domain and solved through a rigorous analytical derivation. Despite the complexity of the derivation, the final result is remarkably simple: the optimal activation reconstruction bases are the eigenvectors of an importance-weighted activation covariance matrix $\mathbf{C} = \text{Cov}(\mathbf{y}) \odot \mathbf{M}$, where $\text{Cov}(\mathbf{y})$ is the covariance matrix of the activations, and \mathbf{M} is the gradient-informed importance matrix (Equations (13)–(15)). These eigenvectors yield the weight matrices \mathbf{W}_1 and \mathbf{W}_2 that minimize performance loss. We apply IMPACT to compress a variety of models across diverse datasets and show that it achieves up to 48.6% greater size reduction while maintaining performance comparable to state-of-the-art baselines.

This paper makes the following contributions:

- We introduce IMPACT, a principled theoretical framework that formally characterizes the relationship between activation reconstruction and its effect on model performance. To our knowledge, this is the first framework within the scope of low-rank weight matrix compression that directly links activation reconstruction to model performance.
- We derive a closed-form solution for selecting optimal reconstruction bases using an importance-weighted activation covariance matrix, enabling importance-aware low-rank compression that prioritizes activation dimensions critical to loss minimization.
- We empirically validate IMPACT across a wide range of models and tasks, showing it achieves significantly higher compression rates while maintaining performance comparable to state-of-the-art methods.

2 Related Work

Singular value decomposition (SVD) (Golub and Loan, 1983) is a widely adopted technique for neural network compression, offering low-rank approximations that reduce model size and improve computational efficiency. Prior work has applied SVD to compress various network components—including convolutional layers, recurrent units, and embeddings—across diverse domains such as natural language processing, speech, and vision (Xue et al., 2013; Jaderberg et al., 2014; Denton et al., 2014; Tai et al., 2016; Kim et al., 2016; Lu et al., 2016; Wen et al., 2017; Chen et al., 2018; Acharya et al., 2019; Wang et al., 2021). More recent efforts extend these methods to Transformer-based architectures (Noach and Goldberg, 2020; Huang et al., 2021; Li et al., 2023; Lv et al., 2023; Sharma et al., 2024), targeting attention and feedforward layers to improve memory and compute efficiency.

Conventional SVD-based approaches minimize weight reconstruction error by retaining the top singular components of weight matrices. However, this strategy may overlook components critical to model performance. To mitigate this, FWSVD (Hsu et al., 2022)

incorporates Fisher information to guide a weighted low-rank factorization, emphasizing parameters with greater influence on the loss landscape.

An emerging line of work moves beyond weight-centric reconstruction and instead targets the preservation of layer activations (Yu and Wu, 2023; Yuan et al., 2023; Chen et al., 2021b). These approaches are motivated by empirical evidence that activations often exhibit stronger low-rank structure than weights. For instance, AFM (Yu and Wu, 2023) optimizes factorized weight matrices to preserve activation behavior rather than merely approximating the original weights. While such methods show improved empirical performance, they generally treat all activation dimensions uniformly and do not account for the heterogeneous contribution of individual dimensions to the model’s predictive accuracy.

In contrast, our work introduces a principled framework that directly links activation reconstruction to downstream model performance. Rather than uniformly reducing reconstruction error, we prioritize preserving the most prediction-critical components of the activation. To the best of our knowledge, this is the first low-rank weight matrix compression framework that explicitly aligns activation reconstruction objectives with model accuracy.

3 The IMPACT Framework

In this section, we present IMPACT, our activation reconstruction-based model compression framework. IMPACT identifies a set of directions that enable importance-aware activation reconstruction, minimizing compression-induced performance degradation. We first formulate the optimization problem and define the compression directions in Section 3.1, laying the foundation for performance-preserving reconstruction. Sections 3.2 to 3.6 develop a systematic solution by transforming the activation space, deriving optimal directions via constrained optimization, and constructing the compressed model. We follow the denominator-layout differentiation convention (Definition 1 in Appendix A) throughout our derivation. Section 3.7 provides a complete algorithm and implementation details of the IMPACT framework.

3.1 Defining the Objective Function

Let $\mathbf{y} \in \mathbb{R}^d$ be the activation produced by a specific layer of the model for a single input sample. We aim to identify a set of r orthonormal vectors $\{\mathbf{u}_1, \dots, \mathbf{u}_r\}$ that define the directions used to reconstruct activations. Each vector satisfies $\|\mathbf{u}_k\| = 1$ and $\mathbf{u}_i \perp \mathbf{u}_j$ for $i \neq j$, with indices $i, j, k \in \{1, \dots, r\}$. The reconstructed activation is denoted by $\hat{\mathbf{y}}$.

Our objective is to select $\{\mathbf{u}_k\}$ such that the reconstructed activation $\hat{\mathbf{y}}$ closely approximates the original activation \mathbf{y} while preserving model performance. To this end, we define the following objective function:

$$\min f(\{\mathbf{u}_k\}) = \alpha \mathbb{E}[\|\mathbf{y} - \hat{\mathbf{y}}\|^2] + \beta \mathbb{E}[(\ell(\mathbf{y}) - \ell(\hat{\mathbf{y}}))^2] \quad (1)$$

This objective comprises two terms:

- $\alpha \mathbb{E}[\|\mathbf{y} - \hat{\mathbf{y}}\|^2]$ encourages $\hat{\mathbf{y}}$ to be numerically close to \mathbf{y} .
- $\beta \mathbb{E}[(\ell(\mathbf{y}) - \ell(\hat{\mathbf{y}}))^2]$ penalizes changes in the loss function ℓ due to discrepancies between \mathbf{y} and $\hat{\mathbf{y}}$.

3.2 Bounding the Objective

We now derive an upper bound on the original objective function, providing a more tractable alternative for optimization.

Theorem 1 (Bounding Theorem) *Suppose the loss function ℓ is C^1 -smooth, and the activation dimension is d . The objective function in Equation (1) is upper bounded by:*

$$f(\{\mathbf{u}_k\}) \leq \mathbb{E} \left[\left\| \sqrt{\beta d \mathbb{E} \left[\left(\frac{\partial \ell}{\partial \mathbf{y}} \right)^2 \right]^\top} + \alpha \odot (\mathbf{y} - \hat{\mathbf{y}}) \right\|^2 \right] \quad (2)$$

Proof Performing Taylor expansion on the loss function, we obtain:

$$\ell(\hat{\mathbf{y}}) \approx \ell(\mathbf{y}) + \frac{\partial \ell}{\partial \mathbf{y}}(\hat{\mathbf{y}} - \mathbf{y})$$

The higher-order terms (e.g., second order and beyond) are ignored because they are computationally expensive to estimate and difficult to capture accurately in practical applications. Plugging this into Equation (1), we get the following results:

$$\begin{aligned} f(\{\mathbf{u}_k\}) &\approx \alpha \mathbb{E}[\|\mathbf{y} - \hat{\mathbf{y}}\|^2] + \beta \mathbb{E} \left[\left(\frac{\partial \ell}{\partial \mathbf{y}}(\mathbf{y} - \hat{\mathbf{y}}) \right)^2 \right] \\ &= \alpha \mathbb{E}[\|\mathbf{y} - \hat{\mathbf{y}}\|^2] + \beta d^2 \mathbb{E} \left[\left(\frac{\frac{\partial \ell}{\partial \mathbf{y}}(\mathbf{y} - \hat{\mathbf{y}})}{d} \right)^2 \right] \\ &= \alpha \mathbb{E}[\|\mathbf{y} - \hat{\mathbf{y}}\|^2] + \beta d^2 \mathbb{E} \left[\left(\frac{\sum_{i=1}^d \left(\frac{\partial \ell}{\partial \mathbf{y}} \right)_i (\mathbf{y} - \hat{\mathbf{y}})_i}{d} \right)^2 \right] \\ &\leq \alpha \mathbb{E}[\|\mathbf{y} - \hat{\mathbf{y}}\|^2] + \beta d^2 \mathbb{E} \left[\left(\frac{\sum_{i=1}^d \left| \left(\frac{\partial \ell}{\partial \mathbf{y}} \right)_i (\mathbf{y} - \hat{\mathbf{y}})_i \right|}{d} \right)^2 \right] \end{aligned}$$

Here, subscript i denotes the i th element of a vector; for instance, $(\mathbf{y} - \hat{\mathbf{y}})_i$ refers to the i th element of $(\mathbf{y} - \hat{\mathbf{y}})$. The second term corresponds to the square of the arithmetic mean of d subterms, which can be upper bounded by the square of their quadratic mean. By applying the QM–AM inequality (Property 1 in Appendix A), we obtain:

$$\begin{aligned} f(\{\mathbf{u}_k\}) &\leq \alpha \mathbb{E}[\|\mathbf{y} - \hat{\mathbf{y}}\|^2] + \beta d^2 \mathbb{E} \left[\frac{\sum_{i=1}^d \left(\frac{\partial \ell}{\partial \mathbf{y}} \right)_i^2 (\mathbf{y} - \hat{\mathbf{y}})_i^2}{d} \right] \\ &= \alpha \mathbb{E}[\|\mathbf{y} - \hat{\mathbf{y}}\|^2] + \beta d \mathbb{E} \left[\left(\frac{\partial \ell}{\partial \mathbf{y}} \right)^2 (\mathbf{y} - \hat{\mathbf{y}})^2 \right] \\ &\approx \alpha \mathbb{E}[\|\mathbf{y} - \hat{\mathbf{y}}\|^2] + \beta d \mathbb{E} \left[\left(\frac{\partial \ell}{\partial \mathbf{y}} \right)^2 \right] \mathbb{E}[(\mathbf{y} - \hat{\mathbf{y}})^2] \end{aligned}$$

Finally, using the Hadamard product, we get:

$$f(\{\mathbf{u}_k\}) \leq \mathbb{E} \left[\left\| \sqrt{\beta d \mathbb{E} \left[\left(\frac{\partial \ell}{\partial \mathbf{y}} \right)^2 \right]^\top} + \alpha \odot (\mathbf{y} - \hat{\mathbf{y}}) \right\|^2 \right]$$

■

To simplify the expression, we set the parameters α and β as follows without loss of generality:

$$\alpha = \eta, \quad \beta = \frac{1 - \eta}{\mathbb{E} \left[\left\| \frac{\partial \ell}{\partial \mathbf{y}} \right\|^2 \right]}$$

where parameter $\eta \in [0, 1]$. The upper bound becomes:

$$h(\{\mathbf{u}_k\}) = \mathbb{E} \left[\left\| \sqrt{\frac{1 - \eta}{\frac{1}{d} \mathbb{E} \left[\left\| \frac{\partial \ell}{\partial \mathbf{y}} \right\|^2 \right]} \mathbb{E} \left[\left(\frac{\partial \ell}{\partial \mathbf{y}} \right)^2 \right]^\top} + \eta \odot (\mathbf{y} - \hat{\mathbf{y}}) \right\|^2 \right] \quad (3)$$

where \odot denotes the Hadamard (elementwise) product. This gives the inequality:

$$f(\{\mathbf{u}_k\}) \leq h(\{\mathbf{u}_k\})$$

Directly minimizing the objective $f(\{\mathbf{u}_k\})$ under the orthonormal constraints

$$\|\mathbf{u}_k\| = 1, \quad \mathbf{u}_i \perp \mathbf{u}_j \text{ for } i \neq j, \quad i, j, k = 1, \dots, r$$

is analytically challenging. Solving this problem via mathematical programming is computationally prohibitive due to the high dimensionality of the variables $\{\mathbf{u}_k\}$, which scale with the size of the large language model's parameters. To address this challenge, we instead minimize the upper bound $h(\{\mathbf{u}_k\})$ of the original objective, subject to the same orthonormal constraints. This relaxation yields an optimization problem that admits an efficient analytical solution.

3.3 Activation Space Transformation

To minimize the objective $h(\{\mathbf{u}_k\})$ under the orthonormal constraints, we transform the activations into a new space where the optimization problem can be solved analytically. Specifically, we define a transformation coefficient \mathbf{a} as:

$$\mathbf{a} = \sqrt{(1 - \eta) \frac{\mathbb{E} \left[\left(\frac{\partial \ell}{\partial \mathbf{y}} \right)^2 \right]^\top}{\frac{1}{d} \mathbb{E} \left[\left\| \frac{\partial \ell}{\partial \mathbf{y}} \right\|^2 \right]} + \eta} \quad (4)$$

Without loss of generality, we assume that the mean-removed reconstructed activations are given by projecting the original activations (after transformation) onto the subspace spanned by $\{\mathbf{u}_k\}$. Formally, we impose:

$$\mathbf{a} \odot (\hat{\mathbf{y}} - \mathbb{E}[\mathbf{y}]) = \left(\sum_k \mathbf{u}_k \mathbf{u}_k^\top \right) (\mathbf{a} \odot (\mathbf{y} - \mathbb{E}[\mathbf{y}])) \quad (5)$$

Defining the transformed activation as

$$\tilde{\mathbf{y}} = \mathbf{a} \odot (\mathbf{y} - \mathbb{E}[\mathbf{y}])$$

we can rewrite the objective $h(\{\mathbf{u}_k\})$ in a form that depends only on the transformed activation, as stated in the following theorem.

Theorem 2 (Activation Space Transformation Theorem) *Given the transformation $\tilde{\mathbf{y}} = \mathbf{a} \odot (\mathbf{y} - \mathbb{E}[\mathbf{y}])$, the objective $h(\{\mathbf{u}_k\})$ becomes:*

$$h(\{\mathbf{u}_k\}) = \mathbb{E} \left[\tilde{\mathbf{y}}^\top \left(\mathbf{I} - \sum_k \mathbf{u}_k \mathbf{u}_k^\top \right) \tilde{\mathbf{y}} \right] \quad (6)$$

Proof Using the transformation coefficient \mathbf{a} , the upper bound function can be written as

$$h(\{\mathbf{u}_k\}) = \mathbb{E} \left[\|\mathbf{a} \odot (\mathbf{y} - \hat{\mathbf{y}})\|^2 \right] \quad (7)$$

Given the projection condition

$$\mathbf{a} \odot (\hat{\mathbf{y}} - \mathbb{E}[\mathbf{y}]) = \left(\sum_k \mathbf{u}_k \mathbf{u}_k^\top \right) (\mathbf{a} \odot (\mathbf{y} - \mathbb{E}[\mathbf{y}])) ,$$

subtracting $\mathbf{a} \odot (\mathbf{y} - \mathbb{E}[\mathbf{y}])$ on both sides and, after that, multiplying both sides with -1, we have

$$\mathbf{a} \odot (\mathbf{y} - \hat{\mathbf{y}}) = \left(\mathbf{I} - \sum_k \mathbf{u}_k \mathbf{u}_k^\top \right) (\mathbf{a} \odot (\mathbf{y} - \mathbb{E}[\mathbf{y}])) \quad (8)$$

Combining Equations (7) and (8), we obtain:

$$h(\{\mathbf{u}_k\}) = \mathbb{E} \left[\left\| \left(\mathbf{I} - \sum_k \mathbf{u}_k \mathbf{u}_k^\top \right) (\mathbf{a} \odot (\mathbf{y} - \mathbb{E}[\mathbf{y}])) \right\|^2 \right]$$

Given the transformed activation $\tilde{\mathbf{y}} = \mathbf{a} \odot (\mathbf{y} - \mathbb{E}[\mathbf{y}])$, the objective function can be rewritten as:

$$\begin{aligned} h(\{\mathbf{u}_k\}) &= \mathbb{E} \left[\left\| \left(\mathbf{I} - \sum_k \mathbf{u}_k \mathbf{u}_k^\top \right) \tilde{\mathbf{y}} \right\|^2 \right] \\ &= \mathbb{E} \left[\tilde{\mathbf{y}}^\top \left(\mathbf{I} - \sum_k \mathbf{u}_k \mathbf{u}_k^\top \right) \cdot \left(\mathbf{I} - \sum_k \mathbf{u}_k \mathbf{u}_k^\top \right) \tilde{\mathbf{y}} \right] \\ &= \mathbb{E} \left[\tilde{\mathbf{y}}^\top \left(\mathbf{I} - 2 \sum_k \mathbf{u}_k \mathbf{u}_k^\top + \sum_{i,j} \mathbf{u}_i \mathbf{u}_i^\top \mathbf{u}_j \mathbf{u}_j^\top \right) \tilde{\mathbf{y}} \right] \end{aligned}$$

As $\{\mathbf{u}_k\}$ are orthogonal vectors where $\mathbf{u}_i \mathbf{u}_j^\top = 0$ if $i \neq j$, we obtain:

$$\begin{aligned} h(\{\mathbf{u}_k\}) &= \mathbb{E} \left[\tilde{\mathbf{y}}^\top \left(\mathbf{I} - 2 \sum_k \mathbf{u}_k \mathbf{u}_k^\top + \sum_k \mathbf{u}_k \mathbf{u}_k^\top \right) \tilde{\mathbf{y}} \right] \\ &= \mathbb{E} \left[\tilde{\mathbf{y}}^\top \left(\mathbf{I} - \sum_k \mathbf{u}_k \mathbf{u}_k^\top \right) \tilde{\mathbf{y}} \right] \end{aligned}$$

■

3.4 Lagrange Formulation and Derivation

To solve the constrained optimization problem, we apply the method of Lagrange multipliers. Our goal is to minimize the objective $h(\{\mathbf{u}_k\})$ subject to the normalization constraint $\|\mathbf{u}_k\| = 1$, along with the orthogonality constraints. To enforce this, we define the Lagrangian function:

$$L(\{\mathbf{u}_k\}) = h(\{\mathbf{u}_k\}) + \sum_{k=1}^r \lambda_k \left(\mathbf{u}_k^\top \mathbf{u}_k - 1 \right) \quad (9)$$

where λ_k is the Lagrange multiplier associated with the constraint $\mathbf{u}_k^\top \mathbf{u}_k = 1$.

We derive the optimality conditions by taking the derivative of $L(\{\mathbf{u}_k\})$ with respect to each \mathbf{u}_k and setting it to zero:

$$\frac{\partial L}{\partial \mathbf{u}_k} = -2\mathbf{u}_k^\top \mathbb{E} \left[\tilde{\mathbf{y}} \tilde{\mathbf{y}}^\top \right] + 2\lambda_k \mathbf{u}_k^\top = 0 \quad (10)$$

To simplify notation, we define the **importance-weighted activation covariance matrix**:

$$\mathbf{C} = \mathbb{E} \left[\tilde{\mathbf{y}} \tilde{\mathbf{y}}^\top \right] \quad (11)$$

Substituting into Equation (10), the optimality condition becomes:

$$-2\mathbf{u}_k^\top \mathbf{C} + 2\lambda_k \mathbf{u}_k^\top = 0 \quad (12)$$

The following theorem characterizes the structure of \mathbf{C} .

Theorem 3 (Importance-Weighted Activation Covariance Matrix) *The matrix \mathbf{C} is equal to the Hadamard product of the activation covariance matrix $\text{Cov}(\mathbf{y})$ and the gradient-informed importance matrix \mathbf{M} , i.e.,*

$$\mathbf{C} = \text{Cov}(\mathbf{y}) \odot \mathbf{M} \quad (13)$$

where

$$\text{Cov}(\mathbf{y}) = \mathbb{E} \left[(\mathbf{y} - \mathbb{E}[\mathbf{y}])(\mathbf{y} - \mathbb{E}[\mathbf{y}])^\top \right] \quad (14)$$

$$\mathbf{M} = \mathbf{a} \mathbf{a}^\top \quad (15)$$

Proof As the importance-weighted activation covariance matrix \mathbf{C} is given by $\mathbf{C} = \mathbb{E}[\tilde{\mathbf{y}}\tilde{\mathbf{y}}^\top]$, plugging the activation transformation $\tilde{\mathbf{y}} = \mathbf{a} \odot (\mathbf{y} - \mathbb{E}[\mathbf{y}])$ into this expression, matrix \mathbf{C} can be written as:

$$\mathbf{C} = \mathbb{E}\left[(\mathbf{a} \odot (\mathbf{y} - \mathbb{E}[\mathbf{y}])(\mathbf{a} \odot (\mathbf{y} - \mathbb{E}[\mathbf{y}]))^\top\right]$$

The (i, j) th element of \mathbf{C} is:

$$\mathbf{C}_{ij} = \mathbb{E}[a_i(y_i - \mathbb{E}[y_i]) \cdot a_j(y_j - \mathbb{E}[y_j])]$$

where a_i , a_j and y_i and y_j are the i th and j th elements of \mathbf{a} and \mathbf{y} , respectively. Since \mathbf{a} is a deterministic vector, the expectation becomes:

$$\mathbf{C}_{ij} = a_i a_j \mathbb{E}[(y_i - \mathbb{E}[y_i]) \cdot (y_j - \mathbb{E}[y_j])]$$

The term $\mathbb{E}[(y_i - \mathbb{E}[y_i]) \cdot (y_j - \mathbb{E}[y_j])]$ is the (i, j) th element of the covariance matrix $\text{Cov}(\mathbf{y})$, which is given by:

$$\text{Cov}(\mathbf{y}) = \mathbb{E}\left[(\mathbf{y} - \mathbb{E}[\mathbf{y}])(\mathbf{y} - \mathbb{E}[\mathbf{y}])^\top\right]$$

Thus,

$$\mathbf{C}_{ij} = a_i a_j \text{Cov}(\mathbf{y})_{ij}$$

For the gradient-informed importance matrix \mathbf{M} , which is defined as $\mathbf{M} = \mathbf{a}\mathbf{a}^\top$, we have $\mathbf{M}_{ij} = a_i a_j$. Hence, the (i, j) th element of matrix \mathbf{C} can be expressed as

$$\mathbf{C}_{ij} = \mathbf{M}_{ij} \text{Cov}(\mathbf{y})_{ij}$$

Therefore, the importance-weighted activation covariance matrix \mathbf{C} is the Hadamard product of the covariance matrix $\text{Cov}(\mathbf{y})$ and the gradient-informed importance matrix \mathbf{M} :

$$\mathbf{C} = \text{Cov}(\mathbf{y}) \odot \mathbf{M}$$

■

Corollary 1 *The importance-weighted activation covariance matrix \mathbf{C} is positive semidefinite and symmetric.*

Proof The gradient-informed importance matrix \mathbf{M} , which is given by $\mathbf{M} = \mathbf{a}\mathbf{a}^\top$, is positive semidefinite and symmetric. Similarly, the covariance matrix $\text{Cov}(\mathbf{y})$, which is given by

$$\text{Cov}(\mathbf{y}) = \mathbb{E}\left[(\mathbf{y} - \mathbb{E}[\mathbf{y}])(\mathbf{y} - \mathbb{E}[\mathbf{y}])^\top\right],$$

is also positive semidefinite and symmetric. According to the Schur product theorem (Zhang, 2006), the Hadamard product of two positive semidefinite matrices is also positive semidefinite. Therefore, the importance-weighted activation covariance matrix $\mathbf{C} = \mathbf{M} \odot \text{Cov}(\mathbf{y})$ is positive semidefinite and symmetric. ■

To empirically illustrate and validate the importance-aware activation reconstruction enabled by the gradient-informed importance matrix \mathbf{M} , we present visual heatmaps and detailed analysis in Section 4.4.

3.5 Reconstruction Direction

From Equation (12) and the fact that \mathbf{C} is real and symmetric, we have:

$$\mathbf{C}\mathbf{u}_k = \lambda_k\mathbf{u}_k \quad (16)$$

This implies that each reconstruction direction \mathbf{u}_k is an eigenvector of \mathbf{C} . We formalize this result in the following theorem:

Theorem 4 (Reconstruction Direction Theorem) *To minimize the objective $h(\{\mathbf{u}_k\})$ under the orthonormality constraints, the optimal k^{th} reconstruction direction \mathbf{u}_k is the eigenvector corresponding to the k^{th} largest eigenvalue of the importance-weighted activation covariance matrix \mathbf{C} .*

Proof Taking the partial derivative of the Lagrangian function with respect to each reconstruction direction \mathbf{u}_k and setting it to zero yields the optimality condition:

$$\frac{\partial L}{\partial \mathbf{u}_k} = -2\mathbf{u}_k^\top \mathbf{C} + 2\lambda_k \mathbf{u}_k^\top = 0$$

Rearranging this equation and taking the transpose of both sides, we obtain:

$$\mathbf{C}^\top \mathbf{u}_k = \mathbf{u}_k \lambda_k$$

Since the matrix \mathbf{C} is symmetric (as established in Corollary 1), we can tell $\mathbf{C} = \mathbf{C}^\top$. By substituting this property, we arrive at:

$$\mathbf{C}\mathbf{u}_k = \lambda_k\mathbf{u}_k \quad (17)$$

Therefore, reconstruction direction \mathbf{u}_k is an eigenvector of the importance-weighted activation covariance matrix \mathbf{C} .

Next, we prove that this direction is the eigenvector corresponds to the k^{th} largest eigenvalue of \mathbf{C} . From the Equation (6), we get:

$$\begin{aligned} h(\{\mathbf{u}_k\}) &= \mathbb{E}[\tilde{\mathbf{y}}^\top \tilde{\mathbf{y}}] - \mathbb{E}\left[\tilde{\mathbf{y}}^\top \sum_k \mathbf{u}_k \mathbf{u}_k^\top \tilde{\mathbf{y}}\right] \\ &= \mathbb{E}[\tilde{\mathbf{y}}^\top \tilde{\mathbf{y}}] - \sum_k \mathbb{E}[\tilde{\mathbf{y}}^\top \mathbf{u}_k \mathbf{u}_k^\top \tilde{\mathbf{y}}] \\ &= \mathbb{E}[\tilde{\mathbf{y}}^\top \tilde{\mathbf{y}}] - \sum_k \mathbb{E}[\mathbf{u}_k^\top \tilde{\mathbf{y}} \tilde{\mathbf{y}}^\top \mathbf{u}_k] \\ &= \mathbb{E}[\tilde{\mathbf{y}}^\top \tilde{\mathbf{y}}] - \sum_k \mathbf{u}_k^\top \mathbb{E}[\tilde{\mathbf{y}} \tilde{\mathbf{y}}^\top] \mathbf{u}_k \end{aligned}$$

As $\mathbf{C} = \mathbb{E}[\tilde{\mathbf{y}} \tilde{\mathbf{y}}^\top]$,

$$h(\{\mathbf{u}_k\}) = \mathbb{E}[\tilde{\mathbf{y}}^\top \tilde{\mathbf{y}}] - \sum_k \mathbf{u}_k^\top \mathbf{C} \mathbf{u}_k$$

Further based on Equation (17),

$$\begin{aligned} h(\{\mathbf{u}_k\}) &= \mathbb{E}[\tilde{\mathbf{y}}^\top \tilde{\mathbf{y}}] - \sum_k \mathbf{u}_k^\top \mathbf{u}_k \lambda_k \\ &= \mathbb{E}[\tilde{\mathbf{y}}^\top \tilde{\mathbf{y}}] - \sum_k \|\mathbf{u}_k\|^2 \lambda_k \end{aligned}$$

As $\|\mathbf{u}_k\|^2 = 1$,

$$h(\{\mathbf{u}_k\}) = \mathbb{E}[\tilde{\mathbf{y}}^\top \tilde{\mathbf{y}}] - \sum_k \lambda_k$$

To minimize $h(\{\mathbf{u}_k\})$, the term $\sum_k \lambda_k$ must be maximized. Since the importance-weighted activation covariance matrix \mathbf{C} is symmetric and positive semidefinite, its eigenvalues are real and non-negative. Therefore, the maximum value of $\sum_k \lambda_k$ is achieved when λ_k is the k^{th} largest eigenvalues of \mathbf{C} , with \mathbf{u}_k its corresponding eigenvector. \blacksquare

The reconstruction directions $\{\mathbf{u}_k\}_{k=1}^r$ are obtained by selecting and normalizing the top r eigenvectors of \mathbf{C} . These eigenvectors are guaranteed to be orthogonal.

3.6 Compressed Model Representation

After obtaining the reconstruction directions $\{\mathbf{u}_k\}_{k=1}^r$, we construct the compressed model accordingly. Given the relationship between the original activation \mathbf{y} and the reconstructed activation $\hat{\mathbf{y}}$:

$$\mathbf{a} \odot (\hat{\mathbf{y}} - \mathbb{E}[\mathbf{y}]) = \left(\sum_k \mathbf{u}_k \mathbf{u}_k^\top \right) (\mathbf{a} \odot (\mathbf{y} - \mathbb{E}[\mathbf{y}]))$$

and the fact that $\mathbf{y} = \mathbf{W}\mathbf{x} + \mathbf{b}$, where \mathbf{W} and \mathbf{b} are the original layer's weight matrix and bias, we can express the reconstructed activation $\hat{\mathbf{y}}$ as follows:

Theorem 5 (Activation Reconstruction Theorem) *The reconstructed activation $\hat{\mathbf{y}}$, which satisfies the projection condition*

$$\mathbf{a} \odot (\hat{\mathbf{y}} - \mathbb{E}[\mathbf{y}]) = \left(\sum_k \mathbf{u}_k \mathbf{u}_k^\top \right) (\mathbf{a} \odot (\mathbf{y} - \mathbb{E}[\mathbf{y}]))$$

is given by:

$$\hat{\mathbf{y}} = \left[\mathbf{U} \oslash (\mathbf{a} \cdot \mathbf{1}_r^\top) \right] \left[(\mathbf{U} \odot (\mathbf{a} \cdot \mathbf{1}_r^\top))^\top \mathbf{W} \right] \mathbf{x} + \mathbb{E}[\mathbf{y}] + (\mathbf{U} \mathbf{U}^\top \odot (\frac{1}{\mathbf{a}} \cdot \mathbf{a}^\top)) (\mathbf{b} - \mathbb{E}[\mathbf{y}])$$

where $\mathbf{U} = [\mathbf{u}_1, \dots, \mathbf{u}_r]$, $\mathbf{1}_r$ is an r -dimensional column vector of ones, \mathbf{W} and \mathbf{b} are the original layer's weight matrix and bias, \mathbf{x} is the input activation, and \oslash denotes Hadamard (element-wise) division.

Proof Rearranging the projection condition

$$\mathbf{a} \odot (\hat{\mathbf{y}} - \mathbb{E}[\mathbf{y}]) = \left(\sum_k \mathbf{u}_k \mathbf{u}_k^\top \right) (\mathbf{a} \odot (\mathbf{y} - \mathbb{E}[\mathbf{y}])) ,$$

we obtain:

$$\mathbf{a} \odot (\hat{\mathbf{y}} - \mathbb{E}[\mathbf{y}]) = \sum_k \mathbf{u}_k (\mathbf{u}_k \odot \mathbf{a})^\top (\mathbf{y} - \mathbb{E}[\mathbf{y}])$$

Applying the Hadamard division $\odot \mathbf{a}$ to both sides of the equation leads to:

$$\hat{\mathbf{y}} - \mathbb{E}[\mathbf{y}] = \sum_k \mathbf{u}_k (\mathbf{u}_k \odot \mathbf{a})^\top (\mathbf{y} - \mathbb{E}[\mathbf{y}]) \odot \mathbf{a}$$

Since $(\mathbf{u}_k \odot \mathbf{a})^\top$ is a row vector and $(\mathbf{y} - \mathbb{E}[\mathbf{y}])$ is a column vector, $(\mathbf{u}_k \odot \mathbf{a})^\top (\mathbf{y} - \mathbb{E}[\mathbf{y}])$ is a scalar, we have

$$\hat{\mathbf{y}} = \mathbb{E}[\mathbf{y}] + \sum_k (\mathbf{u}_k \odot \mathbf{a}) (\mathbf{u}_k \odot \mathbf{a})^\top (\mathbf{y} - \mathbb{E}[\mathbf{y}])$$

Rewriting the equality, we obtain:

$$\hat{\mathbf{y}} = \mathbb{E}[\mathbf{y}] + (\mathbf{U} \odot (\mathbf{a} \cdot \mathbf{1}_r^\top)) (\mathbf{U} \odot (\mathbf{a} \cdot \mathbf{1}_r^\top))^\top (\mathbf{y} - \mathbb{E}[\mathbf{y}])$$

where $\mathbf{U} = [\mathbf{u}_1, \dots, \mathbf{u}_r]$.

Incorporating the original activation $\mathbf{y} = \mathbf{W}\mathbf{x} + \mathbf{b}$, we obtain:

$$\hat{\mathbf{y}} = \mathbb{E}[\mathbf{y}] + (\mathbf{U} \odot (\mathbf{a} \cdot \mathbf{1}_r^\top)) (\mathbf{U} \odot (\mathbf{a} \cdot \mathbf{1}_r^\top))^\top (\mathbf{W}\mathbf{x} + \mathbf{b} - \mathbb{E}[\mathbf{y}])$$

Expanding the expression, the reconstructed activation satisfies:

$$\begin{aligned} \hat{\mathbf{y}} &= \left[\mathbf{U} \odot (\mathbf{a} \cdot \mathbf{1}_r^\top) \right] \left[(\mathbf{U} \odot (\mathbf{a} \cdot \mathbf{1}_r^\top))^\top \mathbf{W} \right] \mathbf{x} \\ &\quad + \mathbb{E}[\mathbf{y}] + (\mathbf{U} \odot (\mathbf{a} \cdot \mathbf{1}_r^\top)) (\mathbf{U} \odot (\mathbf{a} \cdot \mathbf{1}_r^\top))^\top (\mathbf{b} - \mathbb{E}[\mathbf{y}]) \\ &= \left[\mathbf{U} \odot (\mathbf{a} \cdot \mathbf{1}_r^\top) \right] \left[(\mathbf{U} \odot (\mathbf{a} \cdot \mathbf{1}_r^\top))^\top \mathbf{W} \right] \mathbf{x} + \mathbb{E}[\mathbf{y}] + (\mathbf{U}\mathbf{U}^\top \odot \left(\frac{1}{\mathbf{a}} \cdot \mathbf{a}^\top\right)) (\mathbf{b} - \mathbb{E}[\mathbf{y}]) \end{aligned}$$

■

Based on this result, the compressed layer is implemented using two linear layers:

- The first layer has weight matrix

$$\mathbf{W}_1 = (\mathbf{U} \odot (\mathbf{a} \cdot \mathbf{1}_r^\top))^\top \mathbf{W}$$

and no bias;

- The second layer has weight matrix

$$\mathbf{W}_2 = \mathbf{U} \odot (\mathbf{a} \cdot \mathbf{1}_r^\top)$$

and bias

$$\mathbf{b}' = \mathbb{E}[\mathbf{y}] + (\mathbf{U}\mathbf{U}^\top \odot \left(\frac{1}{\mathbf{a}} \cdot \mathbf{a}^\top\right)) (\mathbf{b} - \mathbb{E}[\mathbf{y}])$$

The compressed layer is expressed as:

$$\hat{\mathbf{y}} = \mathbf{W}_2 (\mathbf{W}_1 \mathbf{x}) + \mathbf{b}'$$

3.7 IMPACT Algorithm Description

Algorithm 1 outlines the procedure, which consists of two stages: profiling and compression.

Algorithm 1: IMPACT Algorithm

Input: Model \mathcal{LM}

Output: Compressed Model \mathcal{LM}'

Data: Dataset D , Keeping Ratio k

Stage 1: Profiling;

Let n be the total number of samples in D ;

for each layer l in \mathcal{LM} **do**

Initialize $\mathbb{E}[\mathbf{y}\mathbf{y}^\top]_l = 0$, $\mathbb{E}[\mathbf{y}]_l = 0$, $\mathbb{E}\left[\left(\frac{\partial \ell}{\partial \mathbf{y}}\right)^2\right]_l = 0$;

for each sample $s \in D$ **do**

Get activation \mathbf{y}_l and gradient $\frac{\partial \ell}{\partial \mathbf{y}_l}$ for layer l ;

for each layer l **do**

$\mathbb{E}[\mathbf{y}\mathbf{y}^\top]_l \leftarrow \mathbb{E}[\mathbf{y}\mathbf{y}^\top]_l + \mathbf{y}_l \mathbf{y}_l^\top$;

$\mathbb{E}[\mathbf{y}]_l \leftarrow \mathbb{E}[\mathbf{y}]_l + \mathbf{y}_l$;

$\mathbb{E}\left[\left(\frac{\partial \ell}{\partial \mathbf{y}}\right)^2\right]_l \leftarrow \mathbb{E}\left[\left(\frac{\partial \ell}{\partial \mathbf{y}}\right)^2\right]_l + \left(\frac{\partial \ell}{\partial \mathbf{y}_l}\right)^2$;

for each layer l in **do**

$\mathbb{E}[\mathbf{y}\mathbf{y}^\top]_l \leftarrow \mathbb{E}[\mathbf{y}\mathbf{y}^\top]_l / n$;

$\mathbb{E}[\mathbf{y}]_l \leftarrow \mathbb{E}[\mathbf{y}]_l / n$;

$\text{Cov}(\mathbf{y})_l \leftarrow \mathbb{E}[\mathbf{y}\mathbf{y}^\top]_l - \mathbb{E}[\mathbf{y}]_l \mathbb{E}[\mathbf{y}]_l^\top$;

Stage 2: Compression;

for each layer l **do**

// For brevity, the subscript l is omitted from the notations presented below.

Compute the transformation coefficient \mathbf{a} based on Equation (4);

Compute the gradient-informed importance matrix \mathbf{M} based on Equation (15);

Compute the importance-weighted activation covariance matrix \mathbf{C} based on Equation (13);

$[\mathbf{U}, \mathbf{\Lambda}] = \text{eigenvalue_decomposition}(\mathbf{C})$;

// The columns of \mathbf{U} are the eigenvectors of \mathbf{C} ;

// The vector $\mathbf{\Lambda}$ consists of the eigenvalues of \mathbf{C} ;

Sort the elements of $\mathbf{\Lambda}$ in descending order and reorder \mathbf{U} accordingly;

Find smallest r such that $\left(\sum_{j=1}^r \sqrt{\Lambda_j}\right) / \left(\sum_{j=1}^d \sqrt{\Lambda_j}\right) \geq k/100$;

$\mathbf{U} \leftarrow$ First r columns of \mathbf{U} ;

Substitute the original linear layer with two new linear layers with smaller sizes:

- The first new layer has a weight matrix of $(\mathbf{U} \odot (\mathbf{a} \cdot \mathbf{1}_r^\top))^\top \mathbf{W}$ and no bias;
- The second new layer has a weight matrix of $\mathbf{U} \oslash (\mathbf{a} \cdot \mathbf{1}_r^\top)$ and a bias of $\mathbb{E}[\mathbf{y}] + (\mathbf{U}\mathbf{U}^\top \odot (\frac{1}{\mathbf{a}} \cdot \mathbf{a}^\top))(\mathbf{b} - \mathbb{E}[\mathbf{y}])$;

return Compressed Model \mathcal{LM}' ;

3.7.1 PROFILING STAGE

The algorithm gathers activation and gradient statistics for each linear layer in the model. Specifically, it computes the mean activation, the activation covariance matrix, and the mean squared gradient with respect to the activations. These statistics form the basis for the subsequent compression step.

3.7.2 COMPRESSION STAGE

Using the collected statistics, the algorithm constructs the importance-weighted activation covariance matrix \mathbf{C} for each linear layer by applying a Hadamard product between the activation covariance and the gradient-informed importance matrix. Eigenvalue decomposition is then performed on \mathbf{C} to extract the top eigenvectors, which define the compression directions. Each original linear layer is subsequently replaced by a pair of smaller linear layers designed to preserve model performance.

4 Experiments

4.1 Evaluation Methodology

We evaluate low-rank compression algorithms on two tasks: mathematical reasoning and code generation. For mathematical reasoning, we use the Llama 2-7B and -13B models (Touvron et al., 2023); for code generation, we use CodeLlama-7B and -13B (Roziere et al., 2023). Each model is first finetuned on a task-specific finetuning set, then compressed using a low-rank compression method, and finally undergoes post-compression finetuning before evaluation.

To ensure a fair comparison, we applied the same supervised fine-tuning (SFT) protocol to all methods, including IMPACT and all baselines. We used AdamW with a learning rate of $2e-5$ for Llama 2-7B and CodeLlama-7B, and $1e-5$ for Llama 2-13B and CodeLlama-13B, along with cosine learning rate scheduling (warmup ratio 3%), BF16 mixed precision, and FSDP with LlamaDecoderLayer auto-wrapping. The total batch size was 128 for both Llama 2-7B and CodeLlama-7B (2 GPUs \times 64 samples per GPU), and for Llama 2-13B and CodeLlama-13B (4 GPUs \times 32 samples per GPU). Fine-tuning was performed for 3 epochs on the 7B models and 5 epochs on the 13B models.

For the mathematical reasoning task, we evaluate on GSM8K (Cobbe et al., 2021) and Hendrycks’ MATH (Hendrycks et al., 2021). For code generation, we use MBPP (Austin et al., 2021) and HumanEval (Chen et al., 2021a) as evaluation sets.

We compare our proposed method, IMPACT, against state-of-the-art low-rank compression techniques, including SVD (Xue et al., 2013; Wang et al., 2021; Noach and Goldberg, 2020; Huang et al., 2021; Li et al., 2023; Lv et al., 2023; Sharma et al., 2024; Lin et al., 2025), a widely used matrix factorization method; FWSVD (Hsu et al., 2022), which incorporates weight importance; and AFM (Yu and Wu, 2023), which performs activation-aware weight matrix compression.

Beyond low-rank methods, we also benchmark IMPACT against compression techniques from other paradigms, including QLoRA (Dettmers et al., 2023), a quantization-based approach that finetunes low-rank adapters, and FLAP (An et al., 2024), a pruning method that removes weights based on magnitude and activation variance. These comparisons highlight IMPACT’s robustness and effectiveness across diverse compression strategies.

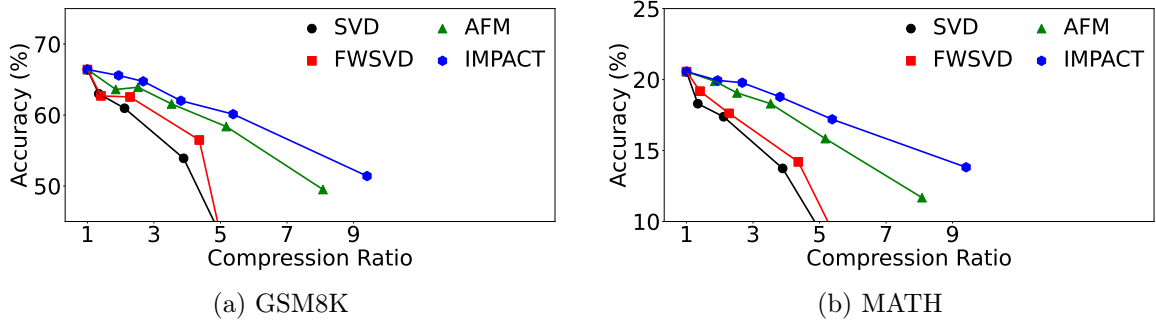


Figure 2: Pass@1 accuracy and model size of Llama 2-7B compressed with various low-rank algorithms on the mathematical reasoning task. Exact values are listed in Table 3 in Appendix B.

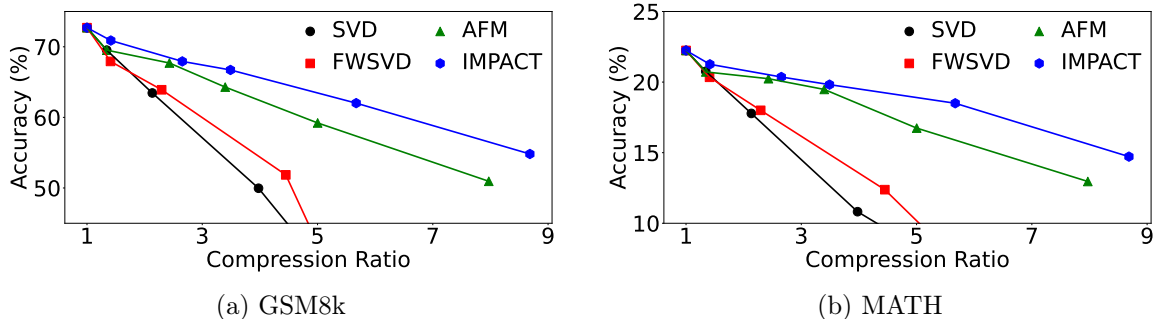


Figure 3: Pass@1 accuracy and model size of Llama 2-13B compressed with various low-rank algorithms on the mathematical reasoning task. Exact values are listed in Table 5 in Appendix B.

4.2 Evaluation of Low-Rank Compression for Mathematical Reasoning

Figures 2 and 3 show the performance of various low-rank compression methods on Llama2-7B and -13B for the mathematical reasoning task. We evaluate the Pass@1 accuracy of the models across a range of compression ratios (the ratio of the original model size to the compressed model size). Our proposed method, IMPACT, consistently outperforms SVD, FWSVD, and AFM across all compression ratios, achieving greater compression while maintaining comparable or superior accuracy.

On Llama 2-7B, IMPACT achieves up to 48.6% greater size reduction than the best-performing baseline (AFM) on GSM8K, and up to 33.4% more on MATH, while maintaining same accuracy.² Across all evaluated compression ratios, it compresses the model over 40% more than SVD and FWSVD on both datasets while delivering similar or better performance. Similar patterns are observed for Llama 2-13B, where IMPACT achieves up to 30.0% more compression than AFM on GSM8K and 32.3% more on MATH. At compression ratios above 2.5 \times , IMPACT continues to deliver over 40% more compression than SVD and FWSVD on both datasets while maintaining better performance.

2. To quantify compression gains, IMPACT’s size is compared to the smallest baseline model with the same accuracy, with details provided in Tables 4 and 6 in Appendix B for Llama 2-7B and -13B, respectively.

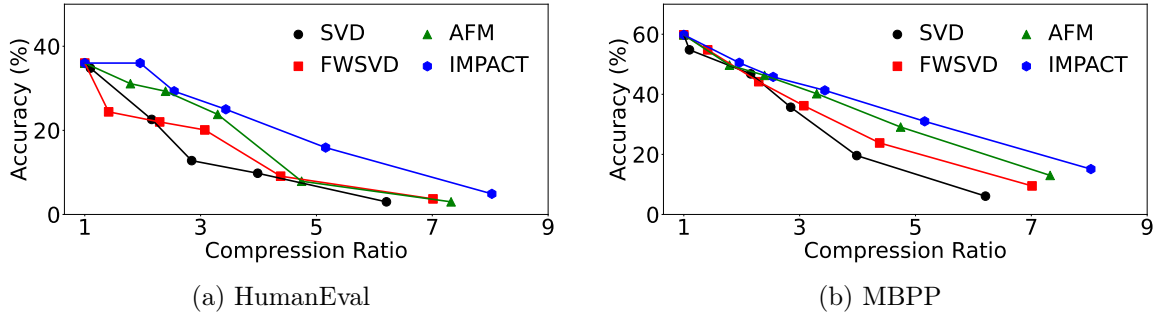


Figure 4: Pass@1 accuracy and model size of CodeLlama-7B compressed with various low-rank algorithms on the code generation task. Exact values are listed in Table 7 in Appendix B.

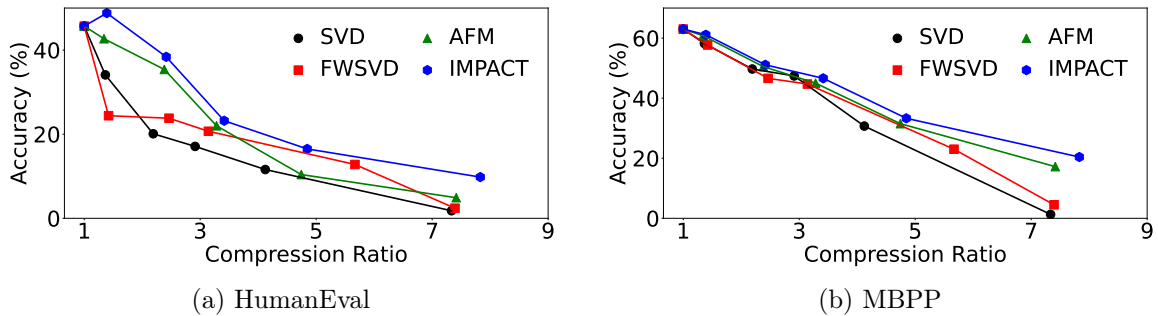


Figure 5: Pass@1 accuracy and model size of CodeLlama-13B compressed with various low-rank algorithms on the code generation task. Exact values are listed in Table 9 in Appendix B.

4.3 Evaluation of Low-Rank Compression for Code Generation

Figures 4 and 5 show the performance of IMPACT and baseline compression methods on CodeLlama-7B and -13B for code generation. We evaluate the Pass@1 accuracy on the HumanEval and MBPP benchmarks across a range of compression ratios.

IMPACT consistently outperforms baseline methods by achieving greater compression while maintaining comparable or superior accuracy on both code generation tasks. On CodeLlama-7B, IMPACT reduces model size by up to 48.9% more than the best-performing baseline on HumanEval, and by 14.8% more on MBPP.³ Similar trends are observed on CodeLlama-13B, where IMPACT achieves up to 28.1% more compression on HumanEval and 15.9% more on MBPP compared to the strongest baseline.

4.4 Visualization and Analysis of the Importance Matrix

To further investigate the mechanism by which IMPACT achieves importance-aware compression, we analyze the structure and statistical properties of the importance matrix \mathbf{M} . While Sections 4.2 and 4.3 quantitatively demonstrate IMPACT’s superior performance, we aim to provide empirical insight into how the model selectively preserves performance-critical components through its use of \mathbf{M} .

3. Tables 8 and 10 in Appendix B provide the details of quantifying IMPACT’s size reduction over the best-performing baselines for CodeLlama-7B and -13B, respectively.

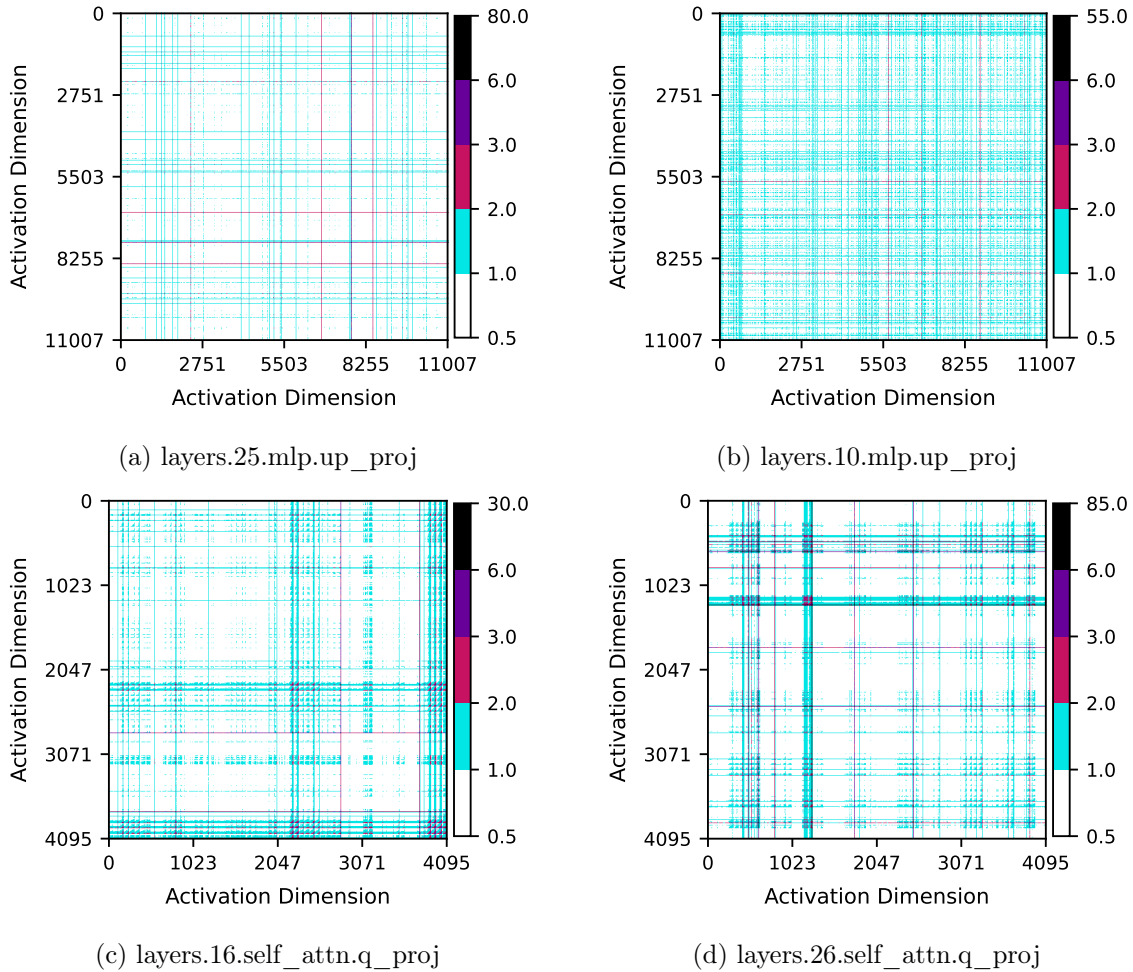


Figure 6: Heatmaps of the importance matrix \mathbf{M} for four representative layers in Llama 2-7B on the mathematical reasoning task (with $\eta = 0.5$). High-intensity rows and columns reflect rare but significant activation dimensions, identified via gradient-based weighting, which IMPACT prioritizes during compression.

We begin by visualizing the structure of \mathbf{M} across four representative layers—two from the MLP modules and two from the attention modules—using the heatmaps in Figure 6. Each heatmap illustrates the values of $\mathbf{M} \in \mathbb{R}^{d \times d}$, where darker entries represent higher importance assigned to particular activation dimension pairs. Across all layers, we observe that a relatively small subset of rows and columns exhibit substantially higher magnitudes, forming localized patterns of elevated intensity. These concentrated regions indicate that IMPACT does not assign importance uniformly across activation dimensions. Instead, the model identifies and emphasizes a sparse set of directions that are deemed more critical to task performance. This selective weighting is central to IMPACT’s design: by constructing the importance-weighted activation covariance matrix $\mathbf{C} = \text{Cov}(\mathbf{y}) \odot \mathbf{M}$, the resulting eigendecomposition yields basis vectors that preferentially preserve high-importance directions during compression.

Complementing the structural visualization, Figure 7 presents the distribution of values in \mathbf{M} for the same layers. These histograms, plotted on a log scale, reveal highly skewed

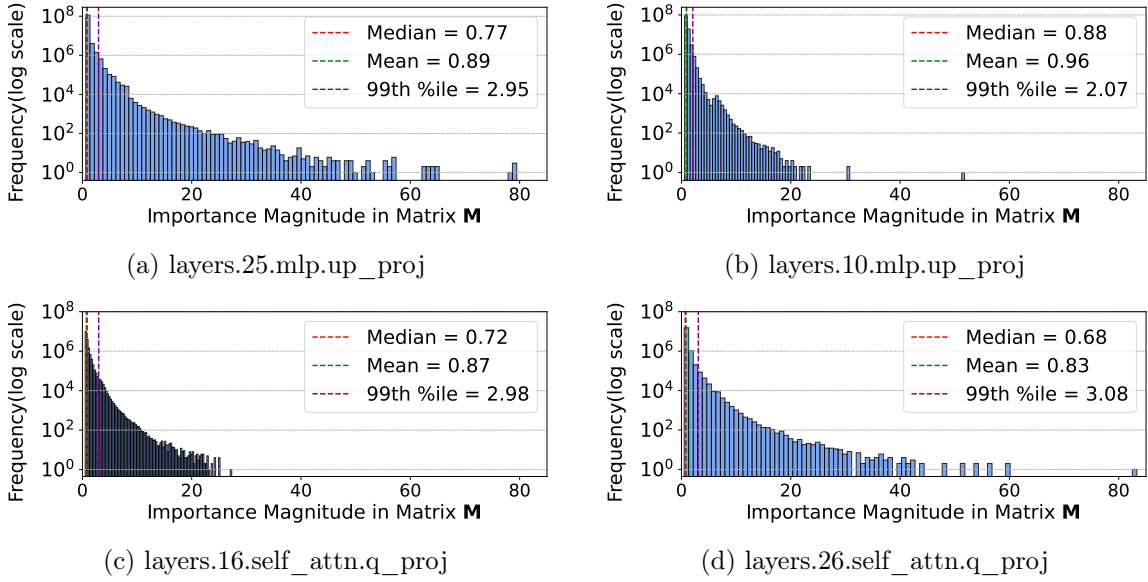


Figure 7: Log-scale histograms of values in the importance matrix \mathbf{M} (with $\eta = 0.5$) for four representative layers of Llama 2-7B on the mathematical reasoning task.

distributions. Although most entries in \mathbf{M} are small, a long tail of large values persists. For instance, in "layers.25.mlp.up_proj", the median of the entries is 0.77, the mean is 0.89, the 99th percentile reaches 2.95, and the maximum is closed to 80. These values quantify the relative importance of preserving interactions between activation dimensions, as determined by their gradient sensitivity during profiling. The long-tailed distribution indicates that IMPACT selectively amplifies a small subset of critical interactions. This pattern is consistent across layers and mirrors the sparsity observed in the heatmaps, reinforcing the model’s emphasis on performance-relevant components.

4.5 Integrating IMPACT with Quantization

Quantization and low-rank compression are distinct model compression techniques grounded in different principles: quantization reduces the precision of model weights, whereas low-rank compression approximates weight matrices as the product of smaller matrices. Quantization generally preserves performance at 8-bit precision or higher but often degrades accuracy at

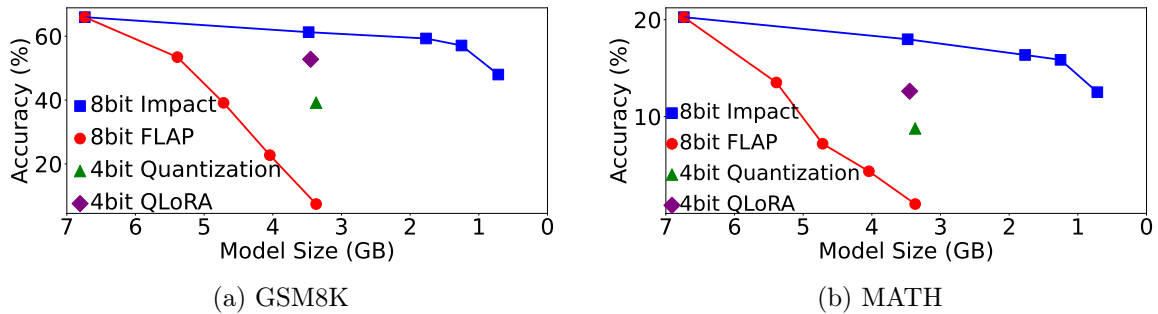


Figure 8: Pass@1 accuracy and model size of Llama 2-7B models compressed using quantization alone, as well as in combination with low-rank compression or pruning techniques, evaluated on the mathematical reasoning task.

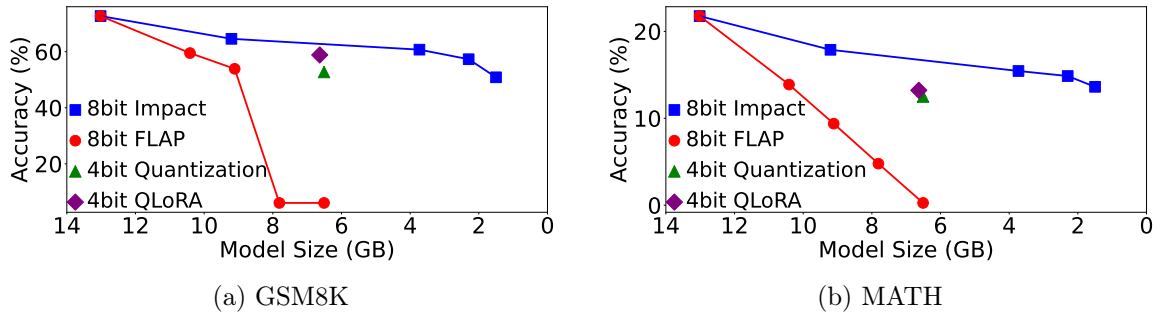


Figure 9: Pass@1 accuracy and model size of Llama 2-13B models compressed using quantization alone, as well as in combination with low-rank compression or pruning techniques, evaluated on the mathematical reasoning task. Tables 1 and 2 present the exact values.

| | | | | | | |
|--------------|-----------------|-------|-------|------|------|------|
| 8-bit FLAP | Model Size (GB) | 6.74 | 5.39 | 4.72 | 4.04 | 3.37 |
| | GSM8K Acc (%) | 66.0 | 53.4 | 39.1 | 22.7 | 7.4 |
| | MATH Acc (%) | 20.3 | 13.5 | 7.2 | 4.4 | 1.0 |
| 8-bit IMPACT | Model Size (GB) | 6.74 | 3.48 | 1.77 | 1.25 | 0.72 |
| | GSM8K Acc (%) | 66.0 | 61.3 | 59.3 | 57.1 | 48.0 |
| | MATH Acc (%) | 20.3 | 18.0 | 16.4 | 15.9 | 12.5 |
| 8-bit FLAP | Model Size (GB) | 13.02 | 10.41 | 9.11 | 7.81 | 6.51 |
| | GSM8K Acc (%) | 72.7 | 59.5 | 53.9 | 6.1 | 6.1 |
| | MATH Acc (%) | 21.8 | 13.9 | 9.4 | 4.8 | 0.3 |
| 8-bit IMPACT | Model Size (GB) | 13.02 | 9.21 | 3.73 | 2.30 | 1.50 |
| | GSM8K Acc (%) | 72.7 | 64.6 | 60.7 | 57.3 | 50.9 |
| | MATH Acc (%) | 21.8 | 17.9 | 15.4 | 14.9 | 13.6 |

Table 1: Pass@1 accuracy and model size of 8-bit-quantized Llama 2-7B and -13B models compressed by FLAP and IMPACT for mathematical reasoning.

| Model Variant | Model Size (GB) | Task | Accuracy (%) |
|---------------------|-----------------|-------|--------------|
| 4-bit-quantized 7B | 3.37 | GSM8K | 39.2 |
| | | MATH | 8.8 |
| 4-bit-QLoRA 7B | 3.45 | GSM8K | 54.1 |
| | | MATH | 12.6 |
| 4-bit-quantized 13B | 6.51 | GSM8K | 52.8 |
| | | MATH | 12.5 |
| 4-bit-QLoRA 13B | 6.63 | GSM8K | 58.8 |
| | | MATH | 13.2 |

Table 2: Pass@1 accuracy and model size of Llama 2-7B and -13B quantized using standard 4-bit quantization and 4-bit QLoRA on the mathematical reasoning task.

lower precisions like 4-bit. To assess the combined effect of quantization and other compression methods such as low-rank compression and pruning, we integrate 8-bit quantization with IMPACT and FLAP to produce compressed models of varying sizes.

Results on the mathematical reasoning task with Llama 2-7B (Figure 8 and Tables 1 and 2) show that IMPACT with 8-bit quantization consistently outperforms pure 4-bit quantization, 4-bit QLoRA, and 8-bit FLAP. At a comparable model size (3.4 GiB), 8-bit IMPACT yields a 53.86% accuracy improvement over 8-bit FLAP and a 7.16% gain over 4-bit QLoRA on GSM8K. Similar trends are observed for Llama 2-13B (Figure 9 and Tables 1 and 2), where 8-bit IMPACT again outperforms all baselines. These results highlight both the superior performance of IMPACT and the benefit of combining low-rank compression with quantization, which yields higher accuracy than either technique alone at the same model size.

4.6 Inference Performance

To evaluate inference performance, we measure the throughput and memory usage of compressed models on the mathematical reasoning task. Figure 10 presents results for models compressed using SVD, FWSVD, AFM, and IMPACT across various model sizes. As expected, larger models exhibit lower throughput and higher memory consumption across all methods. When model size is held constant, all approaches demonstrate comparable throughput and memory consumption. However, because IMPACT achieves similar accuracy at smaller model sizes, it delivers higher throughput and lower memory usage at equivalent accuracy levels. In particular, compared to AFM—the strongest baseline—IMPACT improves throughput by up to 35% and reduces memory consumption by up to 41%.

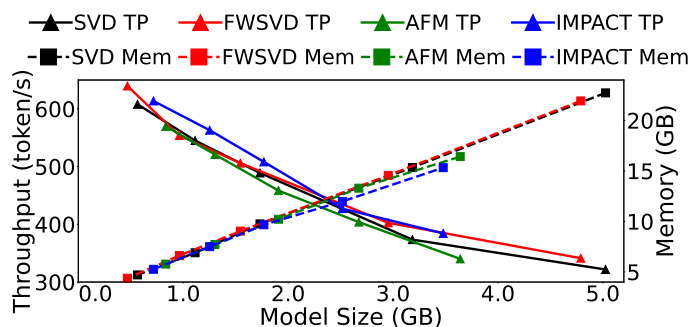


Figure 10: Throughput and memory consumption of compressed models.

5 Conclusion

This paper introduces IMPACT, a principled framework for low-rank model compression that explicitly links activation reconstruction to model performance. In contrast to prior methods that either compress weights directly or minimize activation reconstruction error, IMPACT guides activation reconstruction along directions most critical to model behavior. By formulating and solving a well-grounded optimization problem, we derive a closed-form solution in which the optimal reconstruction bases are the eigenvectors of an importance-weighted activation covariance matrix.

Our empirical results across multiple LLMs and multiple benchmarks demonstrate that IMPACT consistently achieves greater compression—up to 48.6% more than prior state-of-the-art—while maintaining similar accuracy. These findings not only validate the theoretical

underpinnings of our method but also highlight its practical effectiveness for real-world deployment.

IMPACT offers a general and extensible foundation for future compression research. By establishing a formal link between compression decisions and performance outcomes, our work provides both insight and actionable tools for efficient LLM deployment—advancing the broader goal of making powerful models more accessible and sustainable.

Acknowledgments and Disclosure of Funding

This research is funded by a faculty startup grant from Iowa State University. Computational resources are provided by HPC@ISU, which includes equipment funded by the U.S. National Science Foundation under MRI Grant Numbers 1726447 and 2018594.

References

- Anish Acharya, Rahul Goel, Angeliki Metallinou, and Inderjit Dhillon. Online Embedding Compression for Text Classification Using Low Rank Matrix Factorization. In *AAAI Conference on Artificial Intelligence*, 2019.
- Yongqi An, Xu Zhao, Tao Yu, Ming Tang, and Jinqiao Wang. Fluctuation-based Adaptive Structured Pruning for Large Language Models. In *AAAI Conference on Artificial Intelligence*, 2024.
- Jacob Austin, Augustus Odena, Maxwell Nye, Maarten Bosma, Henryk Michalewski, David Dohan, Ellen Jiang, Carrie Cai, Michael Terry, Quoc Le, and Charles Sutton. Program Synthesis with Large Language Models. *arXiv preprint arXiv:2108.07732*, 2021.
- Mark Chen, Jerry Tworek, Heewoo Jun, Qiming Yuan, Henrique Ponde de Oliveira Pinto, Jared Kaplan, Harri Edwards, Yuri Burda, Nicholas Joseph, Greg Brockman, et al. Evaluating Large Language Models Trained on Code. *arXiv preprint arXiv:2107.03374*, 2021a.
- Patrick Chen, Si Si, Yang Li, Ciprian Chelba, and Cho-Jui Hsieh. GroupReduce: Block-Wise Low-Rank Approximation for Neural Language Model Shrinking. In *Conference on Neural Information Processing Systems (NeurIPS)*, 2018.
- Patrick Chen, Hsiang-Fu Yu, Inderjit Dhillon, and Cho-Jui Hsieh. DRONE: Data-Aware Low-Rank Compression for Large NLP Models. In *Conference on Neural Information Processing Systems (NeurIPS)*, 2021b.
- Karl Cobbe, Vineet Kosaraju, Mohammad Bavarian, Mark Chen, Heewoo Jun, Lukasz Kaiser, Matthias Plappert, Jerry Tworek, Jacob Hilton, Reiichiro Nakano, Christopher Hesse, and John Schulman. Training Verifiers to Solve Math Word Problems. *arXiv preprint arXiv:2110.14168*, 2021.
- Emily Denton, Wojciech Zaremba, Joan Bruna, Yann LeCun, and Rob Fergus. Exploiting linear structure within convolutional networks for efficient evaluation. In *Conference on Neural Information Processing Systems (NeurIPS)*, 2014.

- Tim Dettmers, Artidoro Pagnoni, Ari Holtzman, and Luke Zettlemoyer. QLoRA: Efficient Finetuning of Quantized LLMs. In *Conference on Neural Information Processing Systems (NeurIPS)*, 2023.
- Gene H. Golub and Charles F. Van Loan. *Matrix Computations*. Johns Hopkins University Press, 1983. ISBN 978-0-8018-3010-9.
- Dan Hendrycks, Collin Burns, Saurav Kadavath, Akul Arora, Steven Basart, Eric Tang, Dawn Song, and Jacob Steinhardt. Measuring Mathematical Problem Solving with the MATH Dataset. In *Conference on Neural Information Processing Systems (NeurIPS)*, 2021.
- Yen-Chang Hsu, Ting Hua, Sungen Chang, Qian Lou, Yilin Shen, and Hongxia Jin. Language Model Compression with Weighted Low-Rank Factorization. In *International Conference on Learning Representation (ICLR)*, 2022.
- Shaoyi Huang, Shiyang Chen, Hongwu Peng, Daniel Manu, Zhenglun Kong, Geng Yuan, Lei Yang, Shusen Wang, Hang Liu, and Caiwen Ding. HMC-TRAN: A Tensor-core Inspired Hierarchical Model Compression for Transformer-based DNNs on GPU. In *Great Lakes Symposium on VLSI (GLSVLSI)*, 2021.
- Max Jaderberg, Andrea Vedaldi, and Andrew Zisserman. Speeding up Convolutional Neural Networks with Low Rank Expansions. In *British Machine Vision Conference (BMVC)*, 2014.
- Yong-Deok Kim, Eunhyeok Park, Sungjoo Yoo, Taelim Choi, Lu Yang, and Dongjun Shin. Compression of Deep Convolutional Neural Networks for Fast and Low Power Mobile Applications. In Yoshua Bengio and Yann LeCun, editors, *International Conference on Learning Representations (ICLR)*, 2016.
- Hailong Li, Jaewan Choi, Yongsuk Kwon, and Jung Ho Ahn. A Hardware-Friendly Tiled Singular-Value Decomposition-Based Matrix Multiplication for Transformer-Based Models. *IEEE Computer Architecture Letters (CAL)*, 22:169–172, 2023.
- Chi-Heng Lin, Shangqian Gao, James Seale Smith, Abhishek Patel, Shikhar Tuli, Yilin Shen, Hongxia Jin, and Yen-Chang Hsu. MoDeGPT: Modular Decomposition for Large Language Model Compression. In *International Conference on Learning Representations (ICLR)*, 2025.
- Zhiyun Lu, Vikas Sindhvani, and Tara N Sainath. Learning Compact Recurrent Neural Networks. In *IEEE International Conference on Acoustics, Speech and Signal Processing (ICASSP)*, 2016.
- Xiuqing Lv, Peng Zhang, Sunzhu Li, Guobing Gan, and Yueheng Sun. LightFormer: Lightweight Transformer Using SVD-based Weight Transfer and Parameter Sharing. In *Findings of the Association for Computational Linguistics (ACL)*, 2023.
- Matan Ben Noach and Yoav Goldberg. Compressing Pre-trained Language Models by Matrix Decomposition. In *Conference of the Asia-Pacific Chapter of the Association*

for *Computational Linguistics and International Joint Conference on Natural Language Processing (ACL-IJCNLP)*, 2020.

Baptiste Roziere, Jonas Gehring, Fabian Gloeckle, Sten Sootla, Itai Gat, Xiaoqing Ellen Tan, Yossi Adi, Jingyu Liu, Romain Sauvestre, Tal Remez, et al. CodeLlama: Open Foundation Models for Code. *arXiv preprint arXiv:2308.12950*, 2023.

Pratyusha Sharma, Jordan T. Ash, and Dipendra Misra. The Truth is in there: Improving Reasoning in Language Models with Layer-Selective Rank Reduction. In *International Conference on Learning Representations (ICLR)*, 2024.

Cheng Tai, Tong Xiao, Yi Zhang, Xiaogang Wang, and E. Weinan. Convolutional Neural Networks With Low-rank Regularization. In *International Conference on Learning Representations (ICLR)*, 2016.

Hugo Touvron, Louis Martin, Kevin Stone, Peter Albert, Amjad Almahairi, Yasmine Babaei, Nikolay Bashlykov, Soumya Batra, Prajjwal Bhargava, Shruti Bhosale, et al. Llama 2: Open Foundation and Finetuned Chat Models. *arXiv preprint arXiv:2307.09288*, 2023.

Hongyi Wang, Saurabh Agarwal, and Dimitris Papailiopoulos. Pufferfish: Communication-efficient Models at No Extra Cost. In *Conference on Machine Learning and Systems (MLSys)*, 2021.

Wei Wen, Cong Xu, Chunpeng Wu, Yandan Wang, Yiran Chen, and Hai Li. Coordinating Filters for Faster Deep Neural Networks. In *IEEE International Conference on Computer Vision (ICCV)*, 2017.

Jian Xue, Jinyu Li, and Yifan Gong. Restructuring of Deep Neural Network Acoustic Models with Singular Value Decomposition. In *Conference of the International Speech Communication Association (INTERSPEECH)*, January 2013.

Hao Yu and Jianxin Wu. Compressing Transformers: Features Are Low-Rank, But Weights Are Not! In *AAAI Conference on Artificial Intelligence*, 2023.

Zhihang Yuan, Yuzhang Shang, Yue Song, Qiang Wu, Yan Yan, and Guangyu Sun. ASVD: Activation-aware Singular Value Decomposition for Compressing Large Language Models. *arXiv preprint arXiv:2312.05821*, 2023.

Fuzhen Zhang. *The Schur Complement and Its Applications*, volume 4. Springer Science & Business Media, 2006.

Appendix A. Mathematical Preliminaries

Definition 1 (Differentiation Convention) For a differentiable function $\ell(\mathbf{y}) : \mathbb{R}^n \rightarrow \mathbb{R}$ where $\mathbf{y} = [y_1, \dots, y_n]^\top \in \mathbb{R}^n$, the derivative of ℓ with respect to \mathbf{y} following the denominator-layout convention is given by the row vector

$$\frac{\partial \ell}{\partial \mathbf{y}} = \left[\frac{\partial \ell}{\partial y_1} \quad \cdots \quad \frac{\partial \ell}{\partial y_n} \right]$$

We maintain this convention throughout our derivation.

Property 1 (QM-AM Inequality) For set $\{y_i \mid y_i \in \mathbb{R}_{\geq 0}, i = 1, \dots, n\}$, the arithmetic mean (AM) and the quadratic mean (QM) are defined as:

$$\text{AM} = \frac{1}{n} \sum_{i=1}^n y_i, \quad \text{QM} = \sqrt{\frac{1}{n} \sum_{i=1}^n y_i^2}$$

The QM-AM inequality states that: $\text{QM} \geq \text{AM}$, with equality if and only if $y_1 = \dots = y_n$.

Appendix B. Additional Results

| | | | | | | | |
|--------|----------------------|------|------|------|------|------|------|
| SVD | Model Size (Billion) | 6.74 | 5.03 | 3.18 | 1.73 | 1.11 | 0.56 |
| | GSM8K Acc (%) | 66.4 | 63.0 | 61.0 | 53.9 | 32.9 | 11.9 |
| | MATH Acc (%) | 20.6 | 18.3 | 17.4 | 13.7 | 5.3 | 2.8 |
| FWSVD | Model Size (Billion) | 6.74 | 4.79 | 2.95 | 1.54 | 0.96 | 0.47 |
| | GSM8K Acc (%) | 66.4 | 62.7 | 62.5 | 56.5 | 1.5 | 1.9 |
| | MATH Acc (%) | 20.6 | 19.2 | 17.6 | 14.2 | 1.8 | 1.5 |
| AFM | Model Size (Billion) | 6.74 | 3.64 | 2.67 | 1.91 | 1.30 | 0.83 |
| | GSM8K Acc (%) | 66.4 | 63.6 | 63.9 | 61.6 | 58.4 | 49.5 |
| | MATH Acc (%) | 20.6 | 19.9 | 19.1 | 18.3 | 15.8 | 11.7 |
| IMPACT | Model Size (Billion) | 6.74 | 3.48 | 2.52 | 1.77 | 1.25 | 0.72 |
| | GSM8K Acc (%) | 66.4 | 65.6 | 64.7 | 62.0 | 60.1 | 51.4 |
| | MATH Acc (%) | 20.6 | 19.9 | 19.8 | 18.8 | 17.2 | 13.8 |

Table 3: Pass@1 accuracy and model size of Llama 2-7B compressed by various algorithms for the mathematical reasoning task.

| | | GSM8K | | | | | |
|--|----------------------|-------|------|------|------|------|--|
| Best Baseline ⁴ (with Same Acc.) | Model Size (Billion) | 5.82 | 4.90 | 2.06 | 1.63 | 0.93 | |
| | | | | | | | |
| IMPACT | Model Size (Billion) | 3.48 | 2.52 | 1.77 | 1.25 | 0.72 | |
| | Size Reduction (%) | 40.2 | 48.6 | 14.0 | 23.4 | 23.3 | |
| | | MATH | | | | | |
| Best Baseline ⁴ (with Same Acc.) | Model Size (Billion) | 3.91 | 3.52 | 2.39 | 1.64 | 1.07 | |
| | | | | | | | |
| IMPACT | Model Size (Billion) | 3.48 | 2.52 | 1.77 | 1.25 | 0.72 | |
| | Size Reduction (%) | 11.1 | 28.5 | 26.0 | 23.5 | 33.4 | |

Table 4: Size reduction of IMPACT compared to the best baseline at matched accuracy for Llama 2-7B on the mathematical reasoning task.

4. The best baseline refers to the smallest model among SVD, FWSVD, and AFM that achieves accuracy matched to IMPACT. If no baseline exactly matches the accuracy, the model size is interpolated linearly between two adjacent compression points.

| | | | | | | | |
|--------|----------------------|-------|------|------|------|------|------|
| SVD | Model Size (Billion) | 13.02 | 9.70 | 6.10 | 3.27 | 2.07 | 1.01 |
| | GSM8K Acc (%) | 72.7 | 69.5 | 63.5 | 50.0 | 26.9 | 6.7 |
| | MATH Acc (%) | 22.2 | 20.8 | 17.8 | 10.8 | 5.2 | 2.2 |
| FWSVD | Model Size (Billion) | 13.02 | 9.24 | 5.67 | 2.93 | 1.79 | 0.83 |
| | GSM8K Acc (%) | 72.7 | 67.9 | 63.9 | 51.9 | 2.4 | 3.9 |
| | MATH Acc (%) | 22.2 | 20.3 | 18.0 | 12.4 | 1.2 | 1.9 |
| AFM | Model Size (Billion) | 13.02 | 9.69 | 5.36 | 3.83 | 2.60 | 1.63 |
| | GSM8K Acc (%) | 72.7 | 69.5 | 67.7 | 64.3 | 59.2 | 50.9 |
| | MATH Acc (%) | 22.2 | 20.7 | 20.2 | 19.5 | 16.7 | 13.0 |
| IMPACT | Model Size (Billion) | 13.02 | 9.21 | 4.90 | 3.73 | 2.30 | 1.50 |
| | GSM8K Acc (%) | 72.7 | 70.9 | 67.9 | 66.7 | 62.0 | 54.8 |
| | MATH Acc (%) | 22.2 | 21.3 | 20.4 | 19.8 | 18.5 | 14.7 |

Table 5: Pass@1 accuracy and model size of Llama 2-13B compressed by various algorithms for the mathematical reasoning task.

| | | GSM8K | | | | | |
|--|----------------------|-------|------|------|------|------|--|
| Best Baseline ⁴ (with Same Acc.) | Model Size (Billion) | 11.11 | 5.90 | 4.92 | 3.28 | 2.09 | |
| IMPACT | Model Size (Billion) | 9.21 | 4.90 | 3.73 | 2.30 | 1.50 | |
| | Size Reduction (%) | 17.2 | 16.8 | 24.1 | 30.0 | 28.2 | |
| | | MATH | | | | | |
| Best Baseline ⁴ (with Same Acc.) | Model Size (Billion) | 10.82 | 6.44 | 4.51 | 3.39 | 2.08 | |
| IMPACT | Model Size (Billion) | 9.21 | 4.90 | 3.73 | 2.30 | 1.50 | |
| | Size Reduction (%) | 14.9 | 23.8 | 17.4 | 32.3 | 28.1 | |

Table 6: Size reduction of IMPACT compared to the best baseline at matched accuracy for Llama 2-13B on the mathematical reasoning task.

| | | | | | | | |
|--------|----------------------|------|------|------|------|------|------|
| SVD | Model Size (Billion) | 6.74 | 6.14 | 3.13 | 2.37 | 1.69 | 1.09 |
| | HumanEval Acc (%) | 36.0 | 34.8 | 22.6 | 12.8 | 9.8 | 3.0 |
| | MBPP Acc (%) | 59.8 | 54.8 | 46.8 | 35.7 | 19.6 | 6.1 |
| FWSVD | Model Size (Billion) | 6.74 | 4.77 | 2.94 | 2.19 | 1.54 | 0.96 |
| | HumanEval Acc (%) | 36.0 | 24.4 | 22.0 | 20.1 | 9.1 | 3.7 |
| | MBPP Acc (%) | 59.8 | 54.8 | 44.2 | 36.2 | 23.8 | 9.5 |
| AFM | Model Size (Billion) | 6.74 | 3.77 | 2.81 | 2.05 | 1.42 | 0.92 |
| | HumanEval Acc (%) | 36.0 | 31.1 | 29.3 | 23.8 | 7.9 | 3.0 |
| | MBPP Acc (%) | 59.8 | 49.7 | 46.3 | 40.2 | 29.1 | 13.0 |
| IMPACT | Model Size (Billion) | 6.74 | 3.44 | 2.65 | 1.96 | 1.31 | 0.84 |
| | HumanEval Acc (%) | 36.0 | 36.0 | 29.3 | 25.0 | 15.9 | 4.9 |
| | MBPP Acc (%) | 59.8 | 50.5 | 45.8 | 41.3 | 31.0 | 15.1 |

Table 7: Pass@1 accuracy and model size of CodeLlama-7B compressed with various low-rank algorithms on the code generation task.

| HumanEval | | | | | | | |
|--|----------------------|------|------|------|------|------|--|
| Best Baseline ⁴ (with Same Acc.) | Model Size (Billion) | 6.74 | 2.81 | 2.21 | 1.73 | 1.09 | |
| IMPACT | Model Size (Billion) | 3.44 | 2.65 | 1.96 | 1.31 | 0.84 | |
| | Size Reduction (%) | 48.9 | 5.9 | 11.4 | 24.7 | 22.9 | |
| MBPP | | | | | | | |
| Best Baseline ⁴ (with Same Acc.) | Model Size (Billion) | 4.00 | 2.75 | 2.18 | 1.53 | 0.99 | |
| IMPACT | Model Size (Billion) | 3.44 | 2.65 | 1.96 | 1.31 | 0.84 | |
| | Size Reduction (%) | 14.0 | 3.7 | 10.2 | 14.5 | 14.8 | |

Table 8: Size reduction of IMPACT compared to the best baseline at matched accuracy for CodeLlama-7B on the code generation task.

| | | | | | | | |
|--------|----------------------|-------|------|------|------|------|------|
| SVD | Model Size (Billion) | 13.02 | 9.54 | 5.94 | 4.47 | 3.16 | 1.77 |
| | HumanEval Acc (%) | 45.7 | 34.1 | 20.1 | 17.1 | 11.6 | 1.8 |
| | MBPP Acc (%) | 63.0 | 58.2 | 49.7 | 47.4 | 30.7 | 1.3 |
| FWSVD | Model Size (Billion) | 13.02 | 9.17 | 5.29 | 4.14 | 2.30 | 1.76 |
| | HumanEval Acc (%) | 45.7 | 24.4 | 23.8 | 20.7 | 12.8 | 2.4 |
| | MBPP Acc (%) | 63.0 | 57.7 | 46.6 | 44.7 | 23.0 | 4.5 |
| AFM | Model Size (Billion) | 13.02 | 9.71 | 5.47 | 3.97 | 2.74 | 1.76 |
| | HumanEval Acc (%) | 45.7 | 42.7 | 35.4 | 22.0 | 10.4 | 4.9 |
| | MBPP Acc (%) | 63.0 | 60.8 | 50.5 | 45.0 | 31.5 | 17.2 |
| IMPACT | Model Size (Billion) | 13.02 | 9.36 | 5.39 | 3.81 | 2.69 | 1.66 |
| | HumanEval Acc (%) | 45.7 | 48.8 | 38.4 | 23.2 | 16.5 | 9.8 |
| | MBPP Acc (%) | 63.0 | 61.1 | 51.1 | 46.6 | 33.3 | 20.4 |

Table 9: Pass@1 accuracy and model size of CodeLlama-13B compressed with various low-rank algorithms on the code generation task.

| HumanEval | | | | | | | |
|--|----------------------|-------|------|------|------|------|--|
| Best Baseline ⁴ (with Same Acc.) | Model Size (Billion) | 13.02 | 7.21 | 4.10 | 3.16 | 2.14 | |
| IMPACT | Model Size (Billion) | 9.36 | 5.39 | 3.81 | 2.69 | 1.66 | |
| | Size Reduction (%) | 28.1 | 25.2 | 7.0 | 15.0 | 22.4 | |
| MBPP | | | | | | | |
| Best Baseline ⁴ (with Same Acc.) | Model Size (Billion) | 10.16 | 5.71 | 4.40 | 2.91 | 1.98 | |
| IMPACT | Model Size (Billion) | 9.36 | 5.39 | 3.81 | 2.69 | 1.66 | |
| | Size Reduction (%) | 7.8 | 5.6 | 13.4 | 7.6 | 15.9 | |

Table 10: Size reduction of IMPACT compared to the best baseline at matched accuracy for CodeLlama-13B on the code generation task.